In vivo activation of the p53 tumor suppressor pathway by an engineered cyclotide

Yanbin Ji[a], **Subhabrata Majumder**[c], **Melissa Millard**[a], **Radhika Borra**[a], **Tao Bi**[a], **Ahmed Y. Elnagar**[a], **Nouri Neamati**[a], **Alexander Shekhtman**[c], and **Julio A. Camarero**[a,b,2]

[a]Department of Pharmacology and Pharmaceutical Sciences, University of Southern California, Los Angeles, CA 90033, USA

[b]Department of Chemistry, University of Southern California, Los Angeles, CA 90033, USA

[c]Department of Chemistry, State University of New York, Albany, NY 12222, USA

Abstract

The overexpression of Hdm2 and HdmX is a common mechanism used by many tumor cells to inactive the p53 tumor suppressor pathway promoting cell survival. Targeting Hdm2 and HdmX has emerged as a validated therapeutic strategy for treating cancers with wild-type p53. Small linear peptides mimicking the N-terminal fragment of p53 have been shown to be potent Hdm2/HdmX antagonists. The potential therapeutic use of these peptides, however, is limited by their poor stability and bioavailability. Here, we report the engineering of the cyclotide MCoTI-I to efficiently antagonize intracellular p53 degradation. The resulting cyclotide MCo-PMI was able to bind with low nanomolar affinity to both Hdm2 and HdmX, showed high stability in human serum and was cytotoxic to wild-type p53 cancer cell lines by activating the p53 tumor suppressor pathway both *in vitro* and *in vivo*. These features make the cyclotide MCoTI-I an optimal scaffold for targeting intracellular protein-protein interactions.

Keywords

cyclotide; protein engineering; protein interactions; therapeutics

Introduction

The transcription factor p53 plays an essential regulatory role in protecting cells from malignant transformation by inducing cell cycle arrest and apoptosis in response to cellular stress and/or DNA damage.[1,2] The stability and activity of p53 in humans is negatively regulated by the oncogenic proteins Hdm2 and HdmX.[3,4] Both proteins are able to bind the N-terminal region of p53 through p53 binding domains.[5,6] Hdm2 is an E3 ubiquitin ligase that promotes p53 degradation through an ubiquitin-dependent pathway,[2,7] whereas HdmX inhibits p53 transactivation through protein interaction-mediated sequestration.[4,8] The importance of this protective functionality of p53 "as guardian of the genome" is highlighted

by the diversity of molecular strategies used by cancer cells to prevent its activity by promoting deletions, mutations and its sequestration and/or destruction.[9] Hence, the restoration of p53 activity remains an attractive target for the development of more effective cancer therapeutics.[10]

Structural determination of the molecular complex between the transactivation domain of p53 and the p53 binding domains of Hdm2 or HdmX reveals that the protein-protein interaction is mediated by the 15-residue α-helical transactivation domain of p53 that inserts into a hydrophobic cleft on the surface of Hdm2 or HdmX.[6] These findings have lead to the development of a series of small molecules[11] and peptides[12–15] able to antagonize the interaction between p53 and Hdm2 and/or HdmX. Disruption of this interaction stabilizes p53 reducing the viability of cancer cells expressing wild-type p53. Short peptides derived from the transactivation α-helical sequence of p53 and optimized by phage display have been shown to target Hdm2 and HdmX with low nM affinities.[13] Several approaches have been used for the stabilization of the helical structure and improving cell delivery of p53-derived peptides by grafting them onto different protein scaffolds[12,16,17] or by "hydrocarbon stapling".[14] The utility of peptide-based therapeutics, however, has typically been limited by their generally poor stability and limited bioavailability.[18] An exciting approach for improving the stability of peptides is to take advantage of the stability of disulfide rich backbone-cyclized polypeptides.[19] For example several disulfide rich backbone-cyclized polypeptides have been recently used as molecular scaffolds for stabilizing several biologically active short peptides directed against extracellular receptors.[20–23]

Among the different naturally occurring disulfide rich backbone-cyclized polypeptide scaffolds, the cyclotide framework remains one of the most promising for the development of polypeptide-based therapeutics.[24] Cyclotides are a growing new family of plant-derived peptides that share a unique head-to-tail circular knotted topology of three disulfide bridges, with one disulfide penetrating through a macrocycle formed by the other two disulfides and inter-connecting peptide backbones, forming what is called a circular cystine knot (CCK) topology (Fig. 1a). The CCK framework provides a rigid molecular platform[25] with exceptional stability to physical, chemical and biological degradation. For example, some cyclotides have been shown to be orally bioavailable[26] and be able to cross by mammalian cell membranes.[27,28] Recent studies have shown that MCoTI-cyclotides can be uptaken by human cells through macropinocytosis[27,29] although other endocytic mechanisms are also involved depending on the cell type.[27] Cyclotides are also amenable to substantial sequence variation, making them ideal substrates for molecular grafting of biological peptide epitopes.[19,30]

In this work we report for the first time an engineered cyclotide able to modulate an intracellular protein-protein interaction. This cyclotide was designed to antagonize the interaction between p53 and Hdm2/HdmX by grafting a p53-derived helical peptide[13] into one of the loops of the cyclotide *Momordica cochinchinensis* trypsin inhibitor-I (MCoTI-I, Fig. 1a). The resulting cyclotide was able to fold correctly and bind with low nM affinity to the p53 binding domains of both Hdm2 and HdmX. More importantly, the engineered cyclotide showed remarkable stability in human serum and induced cytotoxicity in p53 wild type human cancer cells in a p53-dependent manner both *in vitro* and *in vivo*. Altogether, these results highlight the potential of the cyclotide scaffold in the design of novel peptide-based drug leads for cancer therapy.

Results

Engineering cyclotide MCoTI-I to target p53-Hdm2/HdmX

To engineer the cyclotide MCoTI-I for antagonizing protein-protein interactions between p53 and Hdm2 or HdmX we used the phage-selected α-helical peptide PMI (Fig. 1a).[13] This peptide conserves the residues Phe19, Trp23 and Leu26 of p53 required for the interaction with Hdm2 and HdmX, and is able to bind the p53 binding domains of Hdm2 and Hdmx with low nM affinity.[13] The PMI peptide was grafted onto the cyclotide scaffold using loop 6. This loop has been shown previously to be more disordered in solution[25] and amenable to sequence variation.[31] Interestingly, loop 6 is missing in the STI family suggesting the possibility that long polypeptide sequences could be grafted in this location without disturbing the overall fold of the MCoTI-I scaffold. To facilitate the grafting of the PMI peptide into loop 6 without disturbing its α-helical character or the cyclotide framework, the N-terminus of the PMI peptide was fused to the linker Ala-Ser-Lys/Arg-Ala-Pro (Fig. 1a). This linker is based on the N-terminal region of apamin, a bee-venom neurotoxin that adopts a coil-turn-α-helix structure stabilized by two disulfides.[12] Apamin has also been recently used to correctly display p53-derived helical peptides.[12] Based on this information we hypothesized that grafting of this chimeric peptide will make it possible to display the PMI peptide in the correct biologically active conformation while minimizing the disruption of the cyclotide scaffold. The engineered apamin-PMI hybrid peptide was grafted between residues Ser31 and Gly33 to minimize any possible steric hindrance between the grafted peptide and the MCoTI-I scaffold. The resulting grafted cyclotide was called MCo-PMI (Fig. 1a). We also explored the substitution of the tryptophan residue in the grafted sequence of MCo-PMI by the unnatural amino acid 6-chloro tryptophan to provide the cyclotide MCo-PMI-6W (Fig. 1a).

Replacement of p53 Trp23 by 6-subtituted tryptophan residues has been shown to improve the binding efficiency of p53-derived peptides to Hdm2.[32] Substitution of the residue Phe42 in the PMI segment, which is critical for the interaction with Hdm2 and HdmX,[13] by Ala yielded a negative control for biological experiments.

Production and characterization of MCo-PMI cyclotides

MCoTI-based folded cyclotides were produced either by chemical synthesis or bacterial recombinant expression. Chemical synthesis allowed the introduction of unnatural amino acids, while recombinant expression made possible the production of cyclotides labeled with NMR active isotopes like ^{15}N and ^{13}C to facilitate their structural analysis by heteronuclear NMR. In both cases the backbone cyclization was performed by intramolecular native chemical ligation (NCL) [33–35] using the native Cys located on the beginning of loop 6 to facilitate the cyclization.[31]

Recombinant expression of MCo-based cyclotides was performed by fusing the corresponding linear precursors in frame at the C- and N-terminus to a modified *Mxe* gyrase A intein and a TEV protease recognition sequence, respectively. Once the intein precursor protein was expressed and purified, the N-terminal TEV protease recognition peptide was proteolytically removed. Backbone cyclization and oxidative folding was performed with reduced glutathione (GSH) at physiological pH in one single step (Fig. 1b). Chemical synthesis of the linear precursor peptide thioesters was accomplished using Fmoc-based solid-phase peptide synthesis on a sulfonamide resin. After activation and cleavage of the peptide-resin, the thioester precursors were cyclized and oxidatively folded in one single step with GSH as described above. The cyclization and oxidative folding of MCo-cyclotides was remarkably efficient yielding in both cases the peptide as the major product (Fig. 1b). MCo-cyclotides were purified by preparative reversed-phase (RP)-HPLC and purity

determined by analytical RP-HPLC and electrospray mass spectrometry (ES-MS, Figs. S1 and S2).

Heteronuclear NMR spectroscopy was used to characterize free MCo-PMI (Fig. S3). Comparison between NMR spectra of MCo-PMI and MCoTI-I showed that the cyclotide fold within MCo-PMI is mostly preserved. Changes in chemical shifts are concentrated around loop 6, which accommodates the PMI peptide segment required for the interaction with the p53-binding domains of Hdm2 and HdmX. The differences in chemical shifts between MCo-PMI and MCoTI-I backbone amide protons from loops 1 through 5 are well within 0.2 ppm, indicative of only minor changes in the backbone conformation (Table S3 and Fig. S3). These results are remarkable given the size of the peptide grafted in loop 6 (25 residues versus the original loop sequence containing only 8 residues) and highlight the robustness of this scaffold. The NMR analysis of the cyclotide MCo-PMI segment corresponding to the PMI peptide also reveals that although this segment has a predisposition to adopt -helical conformations as calculated from the NH backbone chemical shifts (Fig. S3G), the absence of a typical -helical Nuclear Overhauser effect (nOe) pattern indicates that it does not adopt a stable helical structure (Fig. S3).

Cyclotide MCo-PMI binds with high affinity to the p53-binding domain of Hdm2 and HdmX

The biological activity of MCo-PMI cyclotides was first tested by fluorescence polarization anisotropy using the p53 binding domains of Hdm2 and HdmX and FITC-labeled derivatives of MCo-PMI-K37R, MCo-PMI-6ClW and MCo-PMI-K37R-F42A (Fig. 2a). FITC was site-specifically incorporated into loop 2 by reacting with the -NH2 group of residue Lys6. Cyclotide MCo-PMI-K37R displayed strong affinity for the p53 binding domain of Hdm2 ($K_D = 2.3 \pm 0.1$ nM) and HdmX ($K_D = 9.7 \pm 0.9$ nM). These affinities are similar to those reported for the peptide PMI[13] thus confirming the PMI peptide segment can adopt a biologically active conformation when grafted onto the cyclotide framework. Intriguingly, the binding affinity of cyclotide MCo-PMI-6W for Hdm2 ($K_D = 2.6 \pm 0.4$ nM) was similar to that of MCo-PMI-K37R suggesting that the replacement of the Trp residue in the PMI peptide is not critical for improving the binding affinity to Hdm2. As expected, cyclotide MCo-PMI-K37R-F42A did not interact with either Hdm2 or HdmX in this dose range (Fig. 2a).

We also performed competition binding assays with unlabeled MCo-PMI cyclotides to test their ability to disrupt the high affinity complexes between the transactivation domain of p53 and Hdm2 or HdmX (Fig. 2b). This was accomplished by using a FRET-based reporter formed by the fluorescent proteins YPet and CyPet fused to a p53 peptide and the p53 binding domains of Hdm2/HdmX respectively. Cyclotides MCo-PMI and MCo-PMI-K37R were able to compete with YPet-p53 for Hdm2 and HdmX binding with similar IC_{50} values (Fig. 2b) indicating that as expected the conservative mutation Lys to Arg did not affect the folding or the biological activity of the resulting cyclotides. All wild-type PMI grafted cyclotides showed IC_{50} values for the inhibition of the p53/HdmX interaction that were around three times higher than those for the inhibition of p53/Hdm2, which is in agreement with the binding affinities shown for the wild-type PMI grafted cyclotides (Fig. 2a) and the values reported for the PMI peptide.[13] Interestingly, wild-type PMI grafted cyclotides were about three times more effective disrupting the p53-Hdm2 complex than the selective Hdm2-inhibitor Nutlin-3. This could be explained in part by the relatively larger interaction surface of the PMI-grafted cyclotide compared to that of the small molecule Nutlin-3. As expected, cyclotides MCoTI-I and MCo-PMI-F42A did not disrupt the interaction between p53 and Hdm2/HdmX. Taken together, these data demonstrate the PMI-grafted cyclotides target both Hdm2 and HdmX *in vitro*, and exhibit only a slight binding preference ($\approx$ 3-fold) for Hdm2 over HdmX.

Cyclotide MCo-PMI targets both intracellular Hdm2 and HdmX

We also investigated the ability of cyclotide MCo-PMI to target intracellular Hdm2 and HdmX. This was accomplished by using co-immunoprecipitation experiments in LNCaP cells. LNCaP cells express wild-type p53 and therefore have been shown to be sensitive to the Hdm2-inhibitor Nutlin-3.[36] LNCaP cells were treated with FITC-labeled cyclotides MCo-PMI-K37R and MCo-PMI-K37R-F42A for 30 h. After cell lysis, FITC-labeled peptides were pulled down using an anti-FITC antibody and the content of proteins Hdm2 and HdmX analyzed by western blotting. Endogenous Hdm2 and HdmX specifically co-inmmuoprecipitated with FITC-labeled MCo-PMI-K37R but not with the inactive mutant MCo-PMI-K37R-F42A (Fig. S8). Fluorescence scanning of the western blot confirmed that in both cases the FITC-labeled cyclotides were able to efficiently penetrate LNCaP cells, therefore confirming that MCo-PMI cyclotide can also target Hdm2 and HdmX within cells.

Cyclotide MCo-PMI is cytotoxic to cancer cells with wild-type p53 expressing Hdm2 and/or HdmX

The ability of the cyclotide MCo-PMI to target intracellular Hdm2 and HdmX prompted us to investigate its effect on cell viability by treating a panel of solid tumor cells expressing wild type p53, and different levels of Hdm2 and/or HdmX. The cell lines used in this study included the Hdm2- and HdmX-expressing prostate and colon cancer cell lines LNCaP and HCT116; and the HdmX-overexpressing human choriocarcinoma cell line JEG-3. In order to study the p53 dependence on the cytotoxic activity of MCo-PMI cyclotides, we used human prostate cancer cell lines PC3 (bearing P274L and V223F p53 mutations) and DU145 (bearing a base pair deletion at codon 138 that generates a stop codon at position 179);[37] and a p53 deficient HCT116 cell line.[38] We also tested breast and kidney epithelial cell lines HBL-100 and HEK293T to evaluate the toxicity of MCo-PMI cyclotides to non-tumorigenic cells.

Cytotoxicity assays were performed by treating cultured cells during 48 h with serial dilutions of Nutlin-3, MCo-PMI, MCo-PMI-F42A and MCoTI-I. Cell viability was measured at the end of the treatment by the MTT assay (Fig. 3). The cyclotide MCoTI-I, used as scaffold to generate grafted PMI cyclotides, showed no detectable cytotoxicity to any of the cells tested in this study up to 100 μM concentration. The lack of cytotoxicity observed in MCoTI-based cyclotides is in agreement with previous reports indicating that these cyclotides are not toxic at concentrations up to 100 μM,[27] confirming the preference of this scaffold for the design of peptide-based therapeutics. The cyclotide MCo-PMI showed dose-dependent cytotoxicity in all the three cell lines tested with wild-type p53 phenotypes, suggesting that MCo-PMI can reactivate the p53 pathway efficiently in cells expressing high levels of Hdm2, HdmX or both (Fig. 3). The most sensitive cell line to MCo-PMI was HCT116 ($EC_{50} \approx 2$ μM), while the HdmX-overexpressing LNCaP and JEG3 cells lines were about 10-fold less sensitive (Fig. 3).

As expected, p53-defficient PC3 and DU145 prostate cancer cell lines were unaffected by MCo-PMI or Nutlin-3 treatments. Genetic deletion of p53 from HCT116 cells also had the same effect. Importantly, we also found that the cyclotide MCo-PMI, showed little cytotoxicity to non-cancerous HBL100 and HEK293T epithelial cells (EC_{50} values 200 μM, Fig. 3). In contrast, Nutlin-3 was moderately cytotoxic to the normal breast epithelial HBL-100 cell line ($EC_{50} = 33 \pm 5$ μM, Fig. 3). It is also worth noting that the mutant cyclotide MCo-PMI-F42A was completely inactive in all the cell lines tested in this work, confirming the specificity and in-cell biological activity of MCo-PMI.

Cyclotide MCo-PMI activates the p53 tumor suppressor pathway

To investigate whether the in-cell biological activity of MCo-PMI was derived from the stabilization of endogenous p53, we treated LNCaP cells for 48 h with vehicle (PBS), Nutlin-3 and cyclotides MCoTI-I, MCo-PMI and MCo-PMI-F42A. The cellular extracts were analyzed by western blotting to visualize the amounts of p53, Hdm2 and HdmX proteins. We also analyzed the intracellular level of p21, which is a regulator of cell-cycle progression at G_1 and is tightly controlled by the tumor suppressor protein p53. Treatment of LNCaP cells with Nutlin-3 (20 μM) and cyclotide MCo-PMI (50 μM) increased the levels of p53 (Fig. 4a). In contrast, treatment with the parent cyclotide MCoTI-I or the inactive MCo-PMI-F42A at the same concentration had little effect on the level of intracellular p53 when compared to the cells treated with vehicle (Fig. 4a). As expected, the level of endogeneous Hdm2 also increased in cells treated with Nutlin-3 or cyclotide MCo-PMI. These results are consistent with an intact p53-Hdm2 counter-regulatory mechanism where Hdm2 transcription and expression is under the control of p53. Likewise, MCo-PMI and Nutlin-3 also induced upregulation of the cyclin-dependent kinase inhibitor p21. The levels of Hdm2 and p21 were unchanged in cells treated with the inactive cyclotide MCo-PMI-F42A when compared to vehicle, hence highlighting the specificity of the cyclotide MCo-PMI to modulate the p53-signaling pathway. Interestingly, the intracellular levels of HdmX were downregulated by cyclotide MCo-PMI, whereas no effect was observed with the inactive mutant MCo-PMI-F42A. This result is consistent with the high affinity of MCo-PMI for both Hdm2 and HdmX, which inhibits binding of endogenous p53 to the Hdm2-HdmX complex preventing its degradation. The stabilization of p53 upregulates the expression of Hdm2, which then can promote ubiquitination and degradation of HdmX.[39]

The upregulation of Hdm2 and p53 showed a dose-dependent relationship with EC_{50} values ≈20 μM (p53) and ≈15 μM (Hdm2) (Fig. 4b), which is consistent with the EC_{50} values obtained in the cell viability assay for this cell line (Fig. 3). The upregulation of p21 and down regulation of HdmX was also dose-dependent with EC_{50} values around 30 μM. To investigate the kinetics of p53 activation, we treated LNCaP cells with 50 μM MCo-PMI for 8 – 48 h and monitored the p53 protein levels by western analysis (Fig. 4c). Cells exposed to MCo-PMI demonstrated increased p53 levels that peaked at 36–48 h post-treatment. A similar trend was also found for the upregulation of Hdm2 and p21, and for the downregulation of HdmX (Fig. 4c).

To determine whether MCo-PMI mediated stabilization of p53 could inhibit cancer cells by reactivating the apoptotic pathway, we performed a caspase-3/7 assay using LNCaP cells treated with MCo-PMI and MCo-PMI-F42A for 30 h (Fig. S9A). Analysis of caspase-3 activation showed that cyclotide MCo-PMI induced dose-dependent caspase-3 activation that could be blocked with a specific caspase-3/7 inhibitor. Cells treated with MCo-PMI-F42A, on the other hand, did not show any caspase-3/7 activity.

We also evaluated cell cycle arrest in LNCaP cells treated with MCo-PMI, MCo-PMI-F42A and Nutlin-3 for 24 h by using the propidium iodide (PI) flow cytometric assay (Fig. S9B). Both, Nutlin-3 and MCo-PMI impeded cell cycle progression, resulting in a depression of the S-phase fraction. This depression was slightly more marked in the cells treated with Nutlin-3. The reduction in the S-phase was associated with accumulation of cells in the G_0/G_1 phase suggesting that the treatment in both cases impedes the cell cycle progression at the G_1/S checkpoint, which is in agreement with the upregulation of p21 observed in cells treated with MCo-PMI and Nutlin-3. Altogether, these data confirm that the in-cell disruption of the p53-Hdm2 and p53-HdmX complexes by MCo-PMI in LNCaP cells leads to the upregulation of p53 transcriptional targets (p21 and Hdm2), caspase-3/7 activation and induction of cell cycle arrest at the G_1/S checkpoint. Interestingly, the upregulation of Hdm2 combined with the inhibition of the interaction between p53 and Hdm2/HdmX also

leads to the downregulation of HdmX likely mediated by the E3-ligase activity of the Hdm2-HdmX complex.[40]

Stability of native, linear and grafted cyclotides

Cyclotide MCoTI-I showed a half-life time of more that 2 days ($t_{1/2} = 55 \pm 5$ h) in human serum at 37° C (Fig. S6A). Naturally occurring MCoTI-cyclotides present a very rigid structure,[25] which makes them remarkably stable to proteolytic degradation. Remarkably, cyclotide MCo-PMI was only slightly less stable ($t_{1/2} = 30 \pm 4$ h) than the parent cyclotide. In contrast, a linearized, reduced and alkylated version of MCo-PMI was rapidly degraded under the same conditions ($t_{1/2} = 0.7 \pm 0.1$ h). The cyclotides MCoTI-I and MCo-PMI were $\approx 80\%$ and 99% bound to serum proteins, respectively, under the conditions employed in our study. We also studied the association and dissociation constant rates of MCo-PMI to human serum proteins. The results indicated that MCo-PMI binds serum proteins with an association and dissociation constant rates of 2.4×10^3 $M^{-1}s^{-1}$ and 2.2×10^{-2} s^{-1}, respectively, which corresponds to a relatively weak dissociation constant of ≈ 10 μM (Fig. S6B).

Suppression of tumor growth by reactivation of the p53 pathway *in vivo*

Encouraged by the previous results, we tested whether the cyclotide MCo-PMI could also modulate the p53 tumor suppressor pathway *in vivo* and therefore inhibit tumor growth. We accomplished this by using a murine xenograft model. HCT116 p53^{+/+} xenografts were established by injecting 0.5×10^6 cells subcutaneously into the rear right flanks of female nuce mice (nu/nu) mice. When the tumor reached an average volume of ≈ 100 mm[3] as determined by caliper measurements, cohorts (n = 3) were treated intravenously with vehicle (5% dextrose in water), MCo-PMI (40 mg/kg, 7.6 mmol/kg), or Nutlin-3 (10 mg/kg, 17.2 mmol/kg) daily for up to 37 days. Treatment with MCo-PMI significantly suppressed tumor growth when compared to animals treated only with vehicle (85% reduction at day 31, p = 0.019) and Nutlin-3 (75% reduction at day 31, p= 0.022) (Fig. 4d). In contrast, animals treated with Nutlin-3 showed only moderate reduction in tumor growth (40% reduction at day 31, p= 0.223) when compared to vehicle (Fig. 4d). At the end of the treatment, the animals were sacrificed and the tumors excised. Snap-frozen tumor samples were analyzed by qRT-PCR using *HDM2* and *P21* primer sets. Treatment of the tumors with MCo-PMI induced a statistically significant transcriptional activation of *HDM2* and *P21* (Fig. 4e). Tumors treated with MCo-PMI peptide showed a marked increase in p53, Hdm2 and p21 expression when compared to vehicle-treated tumors (Figs. 4g-g). Mice treated with MCo-PMI maintained healthy weight throughout treatment and no gross abnormalities were noted in any of the organs or tissues at the time of necropsy (Fig. S7).

Solution structure of MCo-PMI complexed to the p53-binding domain of Hdm2

To better understand the molecular interaction between MCo-PMI and Hdm2/HdmX, we elucidated the three-dimensional structure of the molecular complex between MCo-PMI and Hdm2 (17–116) (Fig. 5). The structure was determined by heteronuclear NMR using ^{15}N-labeled MCo-PMI and ^{13}C,[15]N-labeled Hdm2. The 10 lowest-energy structures (Fig. S3D) are in good agreement with the experimental constraints (Table 1), with no distance and dihedral angle violations over 0.2 Å and 4°, respectively. The solution structure of Hmd2 is in close agreement with the crystal structure of Hdm2 in complex with PMI peptide[13] with a root-mean-square deviation (RMSD) between the Cα atoms is 1.3 Å (Fig. 5c). The overall fold of MCo-PMI conserves the parental Cys-knot topology of MCoTI-I with a more extended loop 6 (Fig. 5). A superimposition of MCoTI-I and MCo-PMI shows RMSD between the Cα atoms in loops 1 through 5 of ≈ 2.0 Å confirming the tolerance of loop 6 to accept long polypeptide grafts. As expected, the helical PMI segment in loop 6 of MCo-PMI

adopts an amphipathic -helical conformation allowing the side-chains of Phe43, Trp47 and Leu50 to bury deep in the p53-binding pocket of Hdm2 (Fig. 5).

MCo-PMI binding to Hdm2 is very similar to that of PMI and other p53-like peptide ligands. The side-chain positions of residues Phe42, Trp46 and Leu49 in MCo-PMI and the equivalent residues in PMI occupy almost identical positions in the complex with Hdm2, and also make identical interactions with the residues of Hdm2 (Fig. 5c). Superimposition of the equivalent C residues of the PMI peptide and PMI segment in MCo-PMI yields an RMSD value of 1.5 Å. The total buried surface area (BSA) contributed by these three residues represents around 34% of the total BSA in the complex. It is worth noting that loop 2 of MCo-PMI is located within van-der-Waals distance to Hdm2 and may favorably contribute to the observed increase in the binding affinity of MCo-PMI for Hdm2 (Fig. 5d). In 9 out of 10 lowest energy structures, negatively charged Asp35 of loop 2 is located within 2 Å from positively charged Lys116 of Hdm2 with the potential of forming a salt bridge that stabilized MCo-PMI-Hdm2 complex (Fig. 5d).

Discussion

Although small peptides mimicking the N-terminal fragment of p53 have been shown to be powerful Hdm2/HdmX antagonists, the use of peptide-based therapeutics is limited by their poor stability and bioavailability. One approach for improving the delivery of specific bioactive peptides to specific targets is the use of disulfide rich backbone-cyclized polypeptides.

In this work we have engineered the cyclotide MCoTI-I to display an -helical peptide derived from the N-terminal fragment of p53 to improve its stability and cellular uptake properties. The resulting cyclotide MCo-PMI was able to bind with low nanomolar affinity to both p53-binding domains of Hdm2 and HdmX, showed high stability in human serum and was cytotoxic to wild-type p53 cancer cell lines both *in vitro* and *in vivo* by activating the p53 tumor suppressor pathway.

The grafted cyclotide MCo-PMI was able to disrupt the interaction between p53 and Hdm2/HdmX both *in vitro* and *in vivo*. Given that both Hdm2 and HdmX bind to the transactivation domain of p53, targeting both p53-binding domains has been shown to be critical for the activation of the p53 tumor suppressor in cancer cells overexpressing Hdm2 and/or HdmX.[14] In agreement with this, the cyclotide MCo-PMI was able to reactivate the p53 tumor suppressor pathway in different cancer lines expressing different levels of Hdm2 and/or HdmX and was not cytotoxic to non-cancer cells or cancer cells with disfunctional p53. Treatment of p53 wild-type cancer cells with the cyclotide MCo-PMI showed upregulation of p53 transcriptional targets confirming in cell activation of the p53 pathway upon treatment. Remarkably, intravenous administration of MCo-PMI to mice bearing an HCT116-xenograft cancer tumor also triggered upregulation of p53 transcriptional targets and suppressed tumor growth. This result is an agreement with the high stability of MCo-PMI in serum and with its ability to reversible bind serum proteins. Although more detailed studies are required to evaluate the potential immunogenicity of particular engineered cyclotides, this is generally considered not to be a major issue for small-sized and stable microproteins.[41,42]

Previous studies have shown that the cyclotides MCoTI-I/II and kalata B1 can be used for introducing novel biological activities.[21,31,43–46] For example, Craik and colleagues have recently grafted peptides fragments (< 10 residues) from the extracellular matrix proteins laminin, osteopontin and VEGF into loop 6 of the cyclotide MCoTI-II and the sunflower trypsin inhibitor-1 (SFTI-1).[21] The grafted cyclotides were considerably more stable in

human serum than the linear grafted peptides and were able to maintain the angiogenic activity (in the nM range) of all linear sequences *in vivo* using a chorioallantoic membrane (CAM) assay. The same group has also reported the engineering of the cyclotide kalata B1 by grafting the Arg-rich peptide epitope (RRKRRR) involved in VEGF-A antagonism onto different loops of the kalata B1.[45] These studies revealed that loops 3 and 6 were the best suited for grafting of the VEGF-A peptide antagonist, while loops 2 and 4 yielded mostly misfolded conformers. The cyclotide engineered in loop 3 was the most active in a cell-based antiangiogenesis assay but showed rather a modest activity ($IC_{50} \approx 12$ μM). The cyclotide kalata B1 used in this work has been reported to be cytotoxic at concentrations above 10 μM. Interestingly, none of the grafted analogues showed the cytoxicity of the parent cyclotide. Tam and colleagues have also used the cyclotide kalata B1 to engineered cyclotides able to antagonize the bradykinin (BK) B_1 receptor.[23] In this work, two short BK-antagonist peptides (<10 residues) were successfully grafted into loop 6 of kalata B1. The resulting cyclotides were biologically active and able to specifically block the BK B_1 receptor in cell assays. The grafted cyclotides were also active *in vivo* showing significant inhibition of pain response in an abdominal constriction animal model assay. Remarkably, the cyclotides were also active when administered orally, while the linearized versions of the cyclotides and the linear grafted peptides showed poor or no inhibition, respectively. This remarkable finding highlights the high stability of the circular cystine-knot topology and its potential to be used as scaffold for the design of orally bioavailable peptide-based drugs. Our group has also recently reported the design of a MCoTI-based cyclotide to target the extracellular cytokine receptor CXCR4.[43] This was accomplished by grafting a topologically modified version of the peptide CVX15, a disulfide cyclic peptide derived from the horseshoe crab peptides polyphemusin-I/II, into loop 6 of the cyclotide MCoTI-I. The most active compound produced in this study was a potent CXCR4 antagonist ($IC_{50} \approx$ 20 nM) and an efficient HIV-1 cell-entry blocker ($IC_{50} \approx 2$ nM). This engineered cyclotide also showed high stability in human serum, thereby providing a promising lead compound for the design of a novel type of peptide-based anticancer and anti-HIV-1 therapeutics. The biological activity of cyclotides can be also modified by introducing single mutations or sequence deletions. For example, Leatherbarrow and colleagues have shown the introduction of a single mutation on the active loop (loop 1) and engineered truncations in loop 6 of cyclotide MCoTI-II resulted in MCoTI-II analogues that showed potent activity against two therapeutically significant serine proteases, -tryptase and human leukocyte elastase.[47]

Here, we show the engineering of a cyclotide that can effectively and selectively target intracellular protein-protein interactions in animal models. Until now, the cyclotide scaffold has been only used to graft small loop- or -hairpin-containing peptide segments[21,44,45] (12 residues long) or introduce point mutations[31,44,46] to introduce new biological activities as mentioned above. In this work we have also demonstrated that by careful design, longer peptides (>20 residues long) containing -helical segments can be engineered into the cyclotide framework. Protein-protein interactions involving -helical segments are quite abundant in nature and therefore this approach should also be valuable for other intracellular targets involving this type of interactions. Moreover, the fact that cyclotides have 5 hypervariable loops opens the possibility for sequence optimization of neighboring loops.

Conclusions

In summary, we have shown that the cyclotide MCoTI-I can be successfully engineered to display and stabilize -helical peptide fragments, and that the resulting cyclotide can be efficiently used both *in vitro* and *in vivo* to target intracellular interactions. These properties make engineered MCo-cyclotides superior in many aspects to existing peptide- or miniprotein-based scaffolds for antagonizing intracellular protein-protein interactions, thus

making this approach extremely valuable in the design of novel peptide-based therapeutic leads.

Supplementary Material

Refer to Web version on PubMed Central for supplementary material.

Acknowledgments

References

(1). Kastan MB, Onyekwere O, Sidransky D, Vogelstein B, Craig RW. Cancer Res. 1991; 51:6304. [PubMed: 1933891]

(2). Levine AJ, Hu W, Feng Z. Cell Death Differ. 2006; 13:1027. [PubMed: 16557269]

(3). Kubbutat MH, Jones SN, Vousden KH. Nature. 1997; 387:299. [PubMed: 9153396]

(4). Shvarts A, Steegenga WT, Riteco N, van Laar T, Dekker P, Bazuine M, van Ham RC, van der Houven van Oordt W, Hateboer G, van der Eb AJ, Jochemsen AG. EMBO J. 1996; 15:5349. [PubMed: 8895579]

(5). Kussie PH, Gorina S, Marechal V, Elenbaas B, Moreau J, Levine AJ, Pavletich NP. Science. 1996; 274:948. [PubMed: 8875929]

(6). Popowicz GM, Czarna A, Holak TA. Cell Cycle. 2008; 7:2441. [PubMed: 18677113]

(7). Tao W, Levine AJ. Proc Natl Acad Sci U S A. 1999; 96:3077. [PubMed: 10077639]

(8). Ohtsubo C, Shiokawa D, Kodama M, Gaiddon C, Nakagama H, Jochemsen AG, Taya Y, Okamoto K. Cancer Sci. 2009; 100:1291. [PubMed: 19432880]

(9). Green DR, Kroemer G. Nature. 2009; 458:1127. [PubMed: 19407794]

(10). Brown CJ, Lain S, Verma CS, Fersht AR, Lane DP. Nat Rev Cancer. 2009; 9:862. [PubMed: 19935675]

(11). Millard M, Pathania D, Grande F, Xu S, Neamati N. Curr Pharm Des. 2011; 17:536. [PubMed: 21391905]

(12). Li C, Pazgier M, Liu M, Lu WY, Lu W. Angew Chem Int Ed Engl. 2009; 48:8712. [PubMed: 19827079]

(13). Pazgier M, Liu M, Zou G, Yuan W, Li C, Li J, Monbo J, Zella D, Tarasov SG, Lu W. Proc Natl Acad Sci U S A. 2009; 106:4665. [PubMed: 19255450]

(14). Bernal F, Wade M, Godes M, Davis TN, Whitehead DG, Kung AL, Wahl GM, Walensky LD. Cancer Cell. 2010; 18:411. [PubMed: 21075307]

(15). Li C, Pazgier M, Yuan W, Liu M, Wei G, Lu WY, Lu W. J Mol Biol. 2010; 398:200. [PubMed: 20226197]

(16). Kritzer JA, Zutshi R, Cheah M, Ran FA, Webman R, Wongjirad TM, Schepartz A. Chembiochem. 2006; 7:29. [PubMed: 16397877]

(17). Li C, Liu M, Monbo J, Zou G, Yuan W, Zella D, Lu WY, Lu W. J Am Chem Soc. 2008; 130:13546. [PubMed: 18798622]

(18). Sanchez-Carbayo M, Socci ND, Lozano JJ, Haab BB, Cordon-Cardo C. Am J Pathol. 2006; 168:93. [PubMed: 16400012]

(19). Garcia AE, Camarero JA. Curr Mol Pharmacol. 2010; 3:153. [PubMed: 20858197]

(20). Clark RJ, Jensen J, Nevin ST, Callaghan BP, Adams DJ, Craik DJ. Angew Chem Int Ed Engl. 2010; 49:6545. [PubMed: 20533477]

(21). Chan LY, Gunasekera S, Henriques ST, Worth NF, Le SJ, Clark RJ, Campbell JH, Craik DJ, Daly NL. Blood. 2011; 118:6709. [PubMed: 22039263]

(22). Aboye TL, Camarero JA. J Biol Chem. 2012; 287:27026. [PubMed: 22707722]

(23). Wong CT, Rowlands DK, Wong CH, Lo TW, Nguyen GK, Li HY, Tam JP. Angew Chem Int Ed Engl. 2012; 51:5620. [PubMed: 22532483]

(24). Gould A, Ji Y, Aboye TL, Camarero JA. Curr Pharm Des. 2011; 17:4294. [PubMed: 22204428]

(25). Puttamadappa SS, Jagadish K, Shekhtman A, Camarero JA. Angew Chem Int Ed Engl. 2010; 49:7030. [PubMed: 20715250]

(26). Saether O, Craik DJ, Campbell ID, Sletten K, Juul J, Norman DG. Biochemistry. 1995; 34:4147. [PubMed: 7703226]

(27). Contreras J, Elnagar AY, Hamm-Alvarez SF, Camarero JA. J Control Release. 2011; 155:134. [PubMed: 21906641]

(28). Cascales L, Henriques ST, Kerr MC, Huang YH, Sweet MJ, Daly NL, Craik DJ. J Biol Chem. 2011; 286:36932. [PubMed: 21873420]

(29). Greenwood KP, Daly NL, Brown DL, Stow JL, Craik DJ. Int J Biochem Cell Biol. 2007; 39:2252. [PubMed: 17693122]

(30). Henriques ST, Craik DJ. Drug Discov Today. 2010; 15:57. [PubMed: 19878736]

(31). Austin J, Wang W, Puttamadappa S, Shekhtman A, Camarero JA. Chembiochem. 2009; 10:2663. [PubMed: 19780078]

(32). Garcia-Echevarria C, Chene P, Blommers MJJ, Furet P. J. Med. Chem. 2000; 43:3205. [PubMed: 10966738]

(33). Dawson PE, Muir TW, Clark-Lewis I, Kent SBH. Science. 1994; 266:776. [PubMed: 7973629]

(34). Camarero JA, Muir TW. Chem. Comm. 1997; 1997:202.

(35). Camarero JA, Pavel J, Muir TW. Angew. Chem. Int. Ed. 1998; 37:347.

(36). Logan IR, McNeill HV, Cook S, Lu X, Lunec J, Robson CN. Prostate. 2007; 67:900. [PubMed: 17440969]

(37). Carroll AG, Voeller HJ, Sugars L, Gelmann EP. Prostate. 1993; 23:123. [PubMed: 8104329]

(38). Bunz F, Hwang PM, Torrance C, Waldman T, Zhang Y, Dillehay L, Williams J, Lengauer C, Kinzler KW, Vogelstein B. J Clin Invest. 1999; 104:263. [PubMed: 10430607]

(39). de Graaf P, Little NA, Ramos YF, Meulmeester E, Letteboer SJ, Jochemsen AG. J Biol Chem. 2003; 278:38315. [PubMed: 12874296]

(40). Wade M, Li YC, Matani AS, Braun SM, Milanesi F, Rodewald LW, Wahl GM. Oncogene. 2012; 31:4789. [PubMed: 22266850]

(41). Craik DJ, Clark RJ, Daly NL. Expert Opin Investig Drugs. 2007; 16:595.

(42). Kolmar H. Curr Opin Pharmacol. 2009; 9:608. [PubMed: 19523876]

(43). Aboye TL, Ha H, Majumder S, Christ F, Debyser Z, Shekhtman A, Neamati N, Camarero JA. J Med Chem. 2012; 55:10729. [PubMed: 23151033]

(44). Huang YH, Colgrave ML, Clark RJ, Kotze AC, Craik DJ. J Biol Chem. 2010; 285:10797. [PubMed: 20103593]

(45). Gunasekera S, Foley FM, Clark RJ, Sando L, Fabri LJ, Craik DJ, Daly NL. J Med Chem. 2008; 51:7697. [PubMed: 19053834]

(46). Thongyoo P, Roque-Rosell N, Leatherbarrow RJ, Tate EW. Org Biomol Chem. 2008; 6:1462. [PubMed: 18385853]

(47). Thongyoo P, Bonomelli C, Leatherbarrow RJ, Tate EW. J Med Chem. 2009; 52:6197. [PubMed: 19772295]
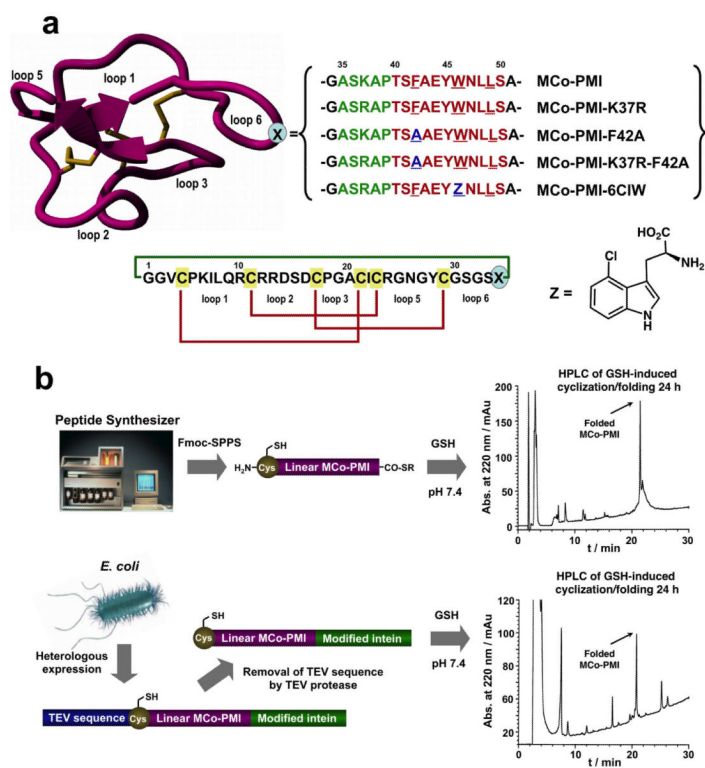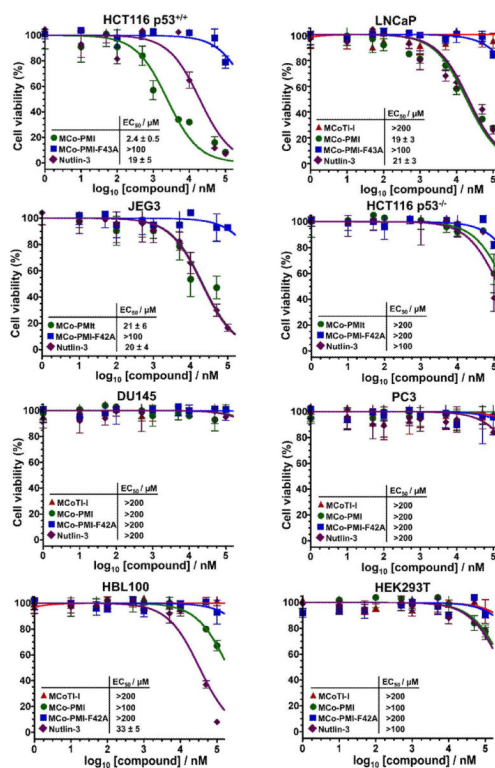
Figure 1.
Design and preparation of the MCo-PMI cyclotides used in this work. **a.** The PMI peptide (red) was grafted onto loop 6 of cyclotide MCoTI-I. To facilitate the insertion of this peptide without disturbing its -helical character or the cyclotide framework, its N-terminus was fused to the apamin-derived linker Ala-Ser-Lys/Arg-Ala-Pro (green). The mutations F42A and W46Z (Z = 6-chloro-tryptophan) are shown in blue. The sequence common to MCoTI-I is shown in black. Conserved cysteine residues are marked in yellow and disulfide connectivities in red. The circular backbone topology is shown with a green line. **b.** Scheme summarizing the approaches used for the chemical synthesis (top) or recombinant production (bottom) of MCo-PMI cyclotides. In both cases the cyclization/folding was performed using an intramolecular version of Native Chemical Ligation in the presence of reduced glutathione (GSH) at pH 7.4. Under these conditions the linear MCo-PMI cyclotide precursors were able to efficiently cyclize and fold in 24 h as shown in the analytical HPLC traces for the crude cyclization/folding reaction for MCo-PMI.
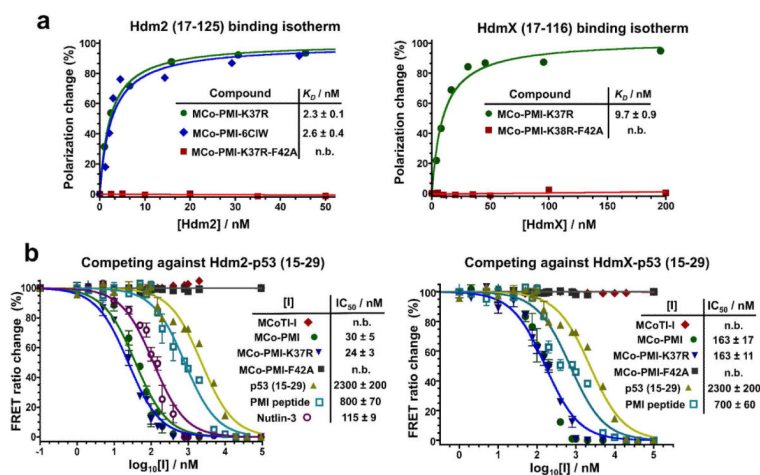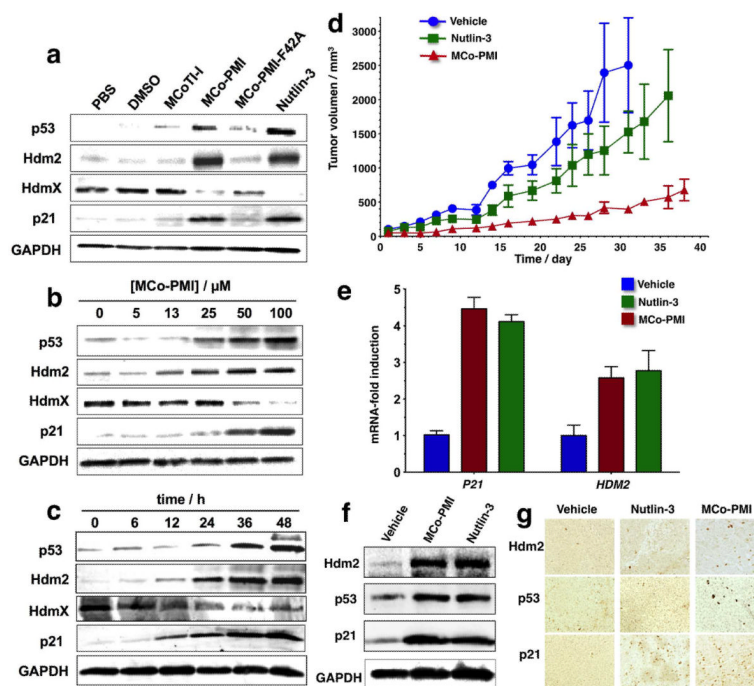
Figure 2.
Binding activities of the MCo-PMI cyclotides. **a.** Direct binding of FITC-labeled MCo-PMI peptides to recombinant Hdm2 (17–125) and HdmX (17–116) was measured by fluorescence polarization anisotropy. **b.** Competition experiments of MCo-PMI peptides and Nutlin-3 with p53 (15–29) for binding to Hdm2 (17–125) and HdmX (17–116). Binding competition experiments were performed by titrating a solution of YPet-p53 (5 μM) and CyPet-Hdm2 (20 nM) or CyPet-HdmX (20 nM) with increasing concentrations of unlabeled inhibitor. The decrease in FRET signal was measured at 525 nm (YPet) by excitation at 414 nm (CyPet). Data are mean ± SEM for experiments performed in triplicate.
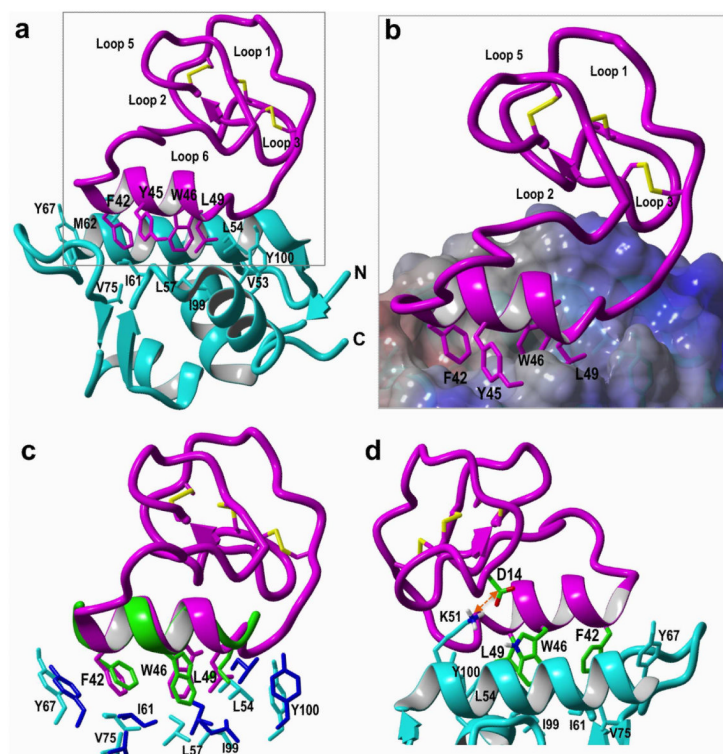
Figure 3.
Cell viability of cancer and normal cells exposed to MCo-PMI cyclotides. Different cancer cell lines expressing different levels of Hdm2 and/or HdmX (HCT116 p53$^{+/+}$, LNCaP and JEG3), non-functional p53 (HCT 116 p53−/−, DU145 and PC3) and non-tumor cells (HBL100 and HEK293T) were treated with 0–100 μM, Nutlin-3, MCo-PMI, MCo-PMI-F42A and/or MCoTI-I for 48 h. Cell viability was assessed by using the MTT assay. Data are mean ± SEM for experiments performed in triplicate.

Figure 4.
Cyclotide MCo-PMI activates the p53 tumor suppressor pathway both *in vitro* and *in vivo*.
a. LNCaP cells were exposed to 50 μM of cyclotides MCo-PMI, MCo-PMI-F42A, MCoTI-I, and Nutlin-3 for 1 h. After 48 h, the soluble cell extracts were analyzed by SDS-PAGE and western blotting for p53, Hdm2, HdmX and p21. **b.** LNCaP cells were exposed to different concentrations of MCo-PMI (0–100 μM) for 48 h. Cell lysates were analyzed for p53, Hdm2, HdmX and p21 as described above. **c.** LNCaP cells were treated with MCo-PMI (50μM) for 1 h. The amount of p53, Hdm2, HdmX and p21 was evaluated by western after 0–48 h of treatment. **d.** Cyclotide MCo-PMI activates the p53 tumor suppressor pathway and blocks tumor growth *in vivo*. Cohorts (N = 3) of HCT116 p53^{+/+} xenografts mice were treated with vehicle (5% dextrose in water), MCo-PMI (40 mg/kg, 7.6 mmol/kg) or Nutlin-3 (10 mg/kg, 17.2 mmol/kg) by intravenous injection daily for up to 38 days. Tumor volume was monitored by caliper measurement. Data are mean ± SEM (day 31: MCo-PMI/vehicle, p = 0.019, MCo-PMI/Nutlin-3, p = 0.022 and Nutlin-3/vehicle, p = 0.223). **e.** Tumors were excised at day 31 (vehicle), day 36 (Nutlin-3) and day 38 (MCo-PMI) and the level of p53 transcriptional targets *HDM2* and *P21* was measured after RNA extraction by qRT-PCR (MCo-PMI/vehicle, p = 0.019, MCo-PMI/Nutlin-3, p = 0.022 and Nutlin-3/vehicle, p = 0.223). Data are mean ± SEM. **f.** Tumors samples were also subjected to SDS-PAGE and analyzed by western blotting for p53, Hdm2 and p21. **g.** The expression level of p53, Hdm2 and p21 was also assessed by immunohistochemical staining. GAPDH was used as loading control in western blots.

Figure 5.
Solution structure of the MCo-PMI and Hdm2 (17–125) complex. **a.** Ribbon representation of MCo-PMI (purple) and Hdm2 (cyan blue) complex. The side-chains of Phe42, Trp46 and Leu49 in MCo-PMI and the Hdm2 residues shaping the hydrophobic binding pocket are shown as sticks in purple and cyan blue respectively. **b.** Close-up view of the binding interface within the Hdm2-MCo-PMI complex. The electrostatic potential at the molecular surface of Hdm2 is shown as positive in blue, negative in red and non-charged in white. **c.** Ribbon representation of the backbone superposition of MCo-PMI (purple) and the PMI peptide (green) (pdb: 3EQS) complexed with Hdm2 (light blue) and Mdm2 (blue), respectively. The key side chains of Phe, Trp and Leu in the MCo-PMI cyclotide and PMI peptide are shown as sticks. The residues lining the cavity of Hdm2 and Mdm2 are also shown. **d.** Close up view of the Hdm2 – MCo-PMI complex reveals and additional salt bridge interaction between Asp35 (MCo-PMI) and Lys51 (Hdm2).

Table 1

NMR and refinement statistics used for the structure calculation of the MCo-PMI - Hdm2 complex

	MCo-PMI	Hdm2
NMR distance and dihedral constraints		
Distance restraints		
Total NOE	357	648
Intra-residue	117	226
Inter-residue	240	422
Sequential ($|i-j|=1$)	114	206
Nonsequential ($|i-j|>1$)	126	216
Hydrogen bonds	22	61
MCo-PMI Hdm2 intermolecular	35	
Total dihedral angle restraints	91	159
φ	45	80
	46	79
Structure statistics		
Violations (mean and s.d.)		
Distance constraints (Å)	0.0153 +/−0.0005	0.0175 +/−0.0024
Dihedral angle constraints (°)	0.5494 +/− 0.3491	
Max. dihedral angle violation (°)	10.3° +/−2.22	
Max. distance constraint violation (Å)	1.03 +/−0.52	
Deviations from idealized geometry		
Bond lengths (Å)	0.001	0.001
Bond angles (°)	0.2	0.2
Average pairwise r.m.s. deviation [*] (Å)		
Heavy	1.67 +/−0.21	
Backbone	1.07 +/−0.14	

[*] Compared to first structure r.m.s deviation was calculated for 10 refined structures.